Supporting Information

Guest-host interactions of nanoconfined anti-cancer drug in metal-organic framework exposed by Terahertz dynamics

Barbara E. Souza,[a] Svemir Rudić,[b] Kirill Titov,[a] Arun S. Babal,[a] James D. Taylor[b] and Jin-Chong Tan*[a]

[a]*Multifunctional Materials & Composites (MMC) Laboratory, Department of Engineering Science, University of Oxford, Parks Road, Oxford OX1 3PJ, UK*
[b]*ISIS Facility, STFC, Rutherford Appleton Laboratory, Chilton, Didcot OX11 0QX, UK*

**jin-chong.tan@eng.ox.ac.uk*

Table of Contents

1. Materials synthesis

1.1. Mechanochemistry of HKUST-1 and encapsulation of 5-FU

The HKUST-1 MOF material was synthesized *via* a manual grinding process. $Cu(NO_3)_3 \cdot 3H_2O$ [copper(II) nitrate trihydrate] (3 mmol) and H_3BTC [benzene-1,3,5-tricarboxylic acid] (2 mmol) were placed in agate mortar and manually ground for 10 min. The product was washed by centrifugation (8000 rpm for 10 min) with methanol to remove unreacted components. HKUST-1 crystals were then dried at room temperature and activated at 100 °C.

Two guest@MOF composite samples were synthesized as follows. For the (one-pot) *in situ* encapsulation of 5-FU, analogous procedure was followed with the addition of 3.5 mmol of 5-FU during the grinding process, producing the 5-FU@HKUST-1_IN particles. *Ex situ* encapsulation of 5-FU was performed by immersion of pre-activated HKUST-1 in a saturated methanolic drug solution under continuous stirring for 48 h. The drug-loaded 5-FU@HKUST-1_EX particles were separated by centrifugation. Pristine HKUST-1 and drug-loaded samples were washed by centrifugation (8000 rpm for 10 min) with methanol and then activated at 90 °C for 12 h in a vacuum oven.

Table S1: Description of samples used in this study.

	Sample	Synthesis method	Drug incorporation strategy
1	HKUST-1	Manual grinding	-
2	5-FU@HKUST-1_IN	Manual grinding	*in situ* encapsulation
3	5-FU@HKUST-1_EX	Manual grinding	*ex situ* encapsulation

2. Materials characterization

2.1. Inelastic neutron scattering

Inelastic neutron scattering (INS) measurements were performed using the TOSCA[1] spectrometer at the ISIS Pulsed Neutron and Muon Source, Rutherford Appleton Laboratory (Chilton, UK). The high-resolution ($\Delta E/E$~1.25%) and broadband (0-4000 cm^{-1}) spectra of each sample (~1 g) were acquired at ~10 K.

TOSCA is an indirect geometry time-of-flight spectrometer where a pulsed, polychromatic beam of neutrons collide with the sample at a distance of ~17 m from the source. The neutrons scattered from the sample were Bragg reflected by a pyrolytic graphite analyser, while higher-order reflections beyond (002) were blocked by a cooled ($T < 30$ K) Beryllium filter in order to define the final energy. Neutrons with final energy of ~32 cm^{-1} were passed towards the detector array composed by thirteen ^3He tubes with effective length of 250 mm. Five banks were located in forward direction (scattering angle ~45°) and five in backwards direction (~135°). The use of a low final energy translated into a direct relationship between energy transfer (E_T, cm^{-1}) and momentum transfer (Q, $Å^{-1}$) such that $E_T \approx 16Q^2$. Energy transfer and spectral intensity, i.e. $S(Q, \omega)$, were then obtained using the Mantid software.[2] Each sample was wrapped in 4 cm × 4.6 cm aluminium sachet and placed into a 2.0 mm spaced flat aluminium cell, which was sealed with indium wire. Sample preparation and cell loading into the cell took place in a glovebox to avoid moisture uptake by the sample. To reduce the effect of the Debye-Waller factor on the experimental spectral intensity and allow comparison with

the theoretical spectra, the sample cell was cooled to ~10 K by a closed cycle refrigerator (CCR). The INS spectra were collected under vacuum over a duration of 4-6 hours.

The neutron guide upgrade of the TOSCA spectrometer, completed in 2017, has increased the neutron flux at the sample position by as much as 82 times. This upgrade improves the performance through faster measurements and by reducing the required sample mass.[3]

2.2. X-ray diffraction

The powder samples were analyzed by X-ray diffraction (XRD) using the Rigaku MiniFlex diffractometer with a Cu K_α source (1.541 Å). Samples were weighed before measurement and diffraction data was collected from 3° to 40°, using a 0.02° step size and 1.0° min^{-1} step speed. The patterns were then normalized with respect to the most intense peak and used for phase identification.

2.3. Thermogravimetric analysis

Thermogravimetric analysis (TGA) was performed using TGA-Q50 (TA instruments). Approximately 4 mg of each sample was placed in a platinum pan (maximum volume 50 μL) and heated from 50 °C to 500 °C with a heating rate of 10 °C min^{-1}. The measurements were performed under a dry nitrogen flow of 40 mL min^{-1}.

2.4. Attenuated total reflectance Fourier transform infrared spectroscopy

Attenuated total reflectance Fourier transform infrared spectroscopy (ATR-FTIR) spectra were acquired at room temperature with a Nicolet iS10 FTIR spectrometer with an ATR sample holder. The spectra were collected in the range of 750-2000 cm^{-1} with a resolution of 0.5 cm^{-1} and normalized in respect to the most intense vibrational peak to facilitate comparison across the different samples under study.

2.5. Scanning electron microscopy and atomic force microscopy

Analyses of the morphology and particle size determination were carried out by scanning electron microscopy (SEM) and atomic force microscopy (AFM). SEM images were obtained using Carl Zeiss EVO LS15 at 15 keV under high vacuum. Atomic force microscopy (AFM) was performed using the Veeco Dimension 3100 AFM equipped with an in-line optical zoom microscope with colour CCD camera for precise placement of probe onto the sample. The microscope was operated under the tapping mode, equipped with a Tap300G silicon probe with resonance frequency of 30 kHz, spring constant of 40 Nm^{-1}, and tip radius < 10 nm.

2.6. Specific surface area measurements

The Brunauer-Emmett-Teller (BET) specific surface area of samples was determined from nitrogen adsorption-desorption isotherms at 77 K, measured with Quantachrome Nova 1200. The isotherms were obtained using a Ø9 mm sample cell containing 60-100 mg of samples under study. The outgassing temperature was 90 °C during sample activation under vacuum.

2.7. Ab initio density functional theory calculations

Density functional theory (DFT) calculations to generate the INS spectra of HKUST-1 were obtained from the work published by Ryder and Tan.[4] The vibrational calculation was carried out at the B3LYP level of theory using the periodic CRYSTAL14 code. We used the DFT

output file of this study to generate the INS spectrum using the Mantid software[2] through the AbINS extension.[5] During the spectrum generation a total cross section was considered with a quantum order events number of 1.

2.8. Calculation of area under INS curve

The Integrate Gadget in OriginPro was used to perform the numerical integration on the INS spectra to determine the area under the curve of specific vibrational modes. The range of data was selected to include the peaks of the vibrational modes of interest, using the *x*-axis as the baseline.

2.9. Release of 5-FU drug molecules (guests) from HKUST-1 host

To perform the release of the guest molecules from the host framework, 20 mg of the drug-loaded composite samples were immersed in abundant methanol and constantly stirred at room temperature for a period of 72 hours. The material was recovered and washed by centrifugation twice with methanol (8000 rpm for 10 min) to guarantee complete removal of guest molecules present in the final composite sample.

2.10. Fabrication of pellets

Pellets were prepared on a standard hydrostatic lab press with a die of 13 mm and under a constant force of 1 ton. The nominal density of each pellet was determined by weighing each one of them and dividing this quantity by its nominal volume. The dimensions of the pellets were determine using a micrometer.

3. Recovery of the pristine crystalline structure

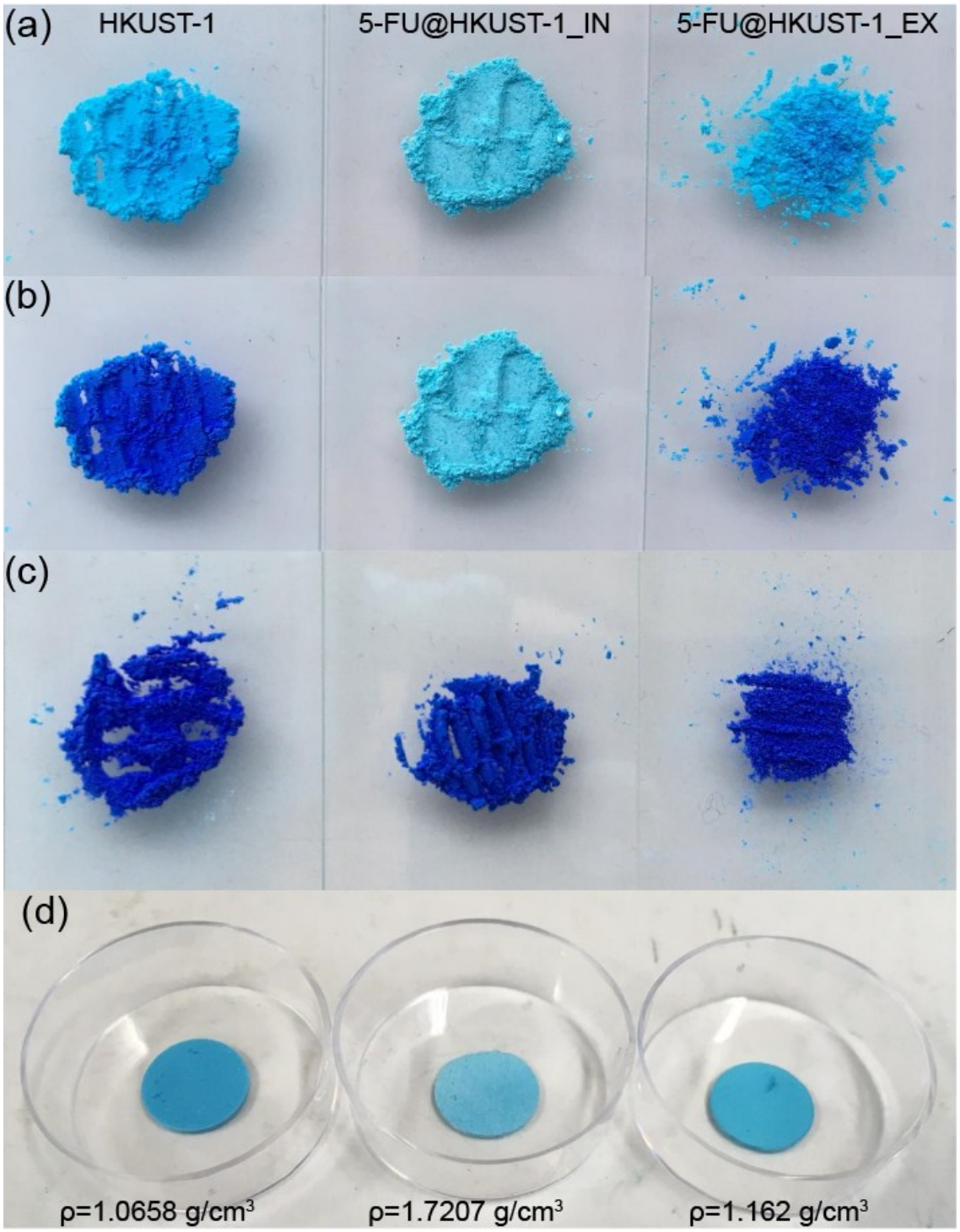

Fig. S1 (a) HKUST-1 (left), 5-FU@HKUST-1_IN (center) and 5-FU@HKUST-1_EX (right) before sample activation. (b) Colour change observed after samples activation at 90 °C under vacuum. HKUST-1 framework presents a characteristic color switch from light to dark blue upon heating, linked to the change in coordination of the copper site. 5-FU@HKUST-1_IN did not present the expected colour change, due to the coordination of the guest molecule to the copper metal site.[6] (c) Colour change presented by all samples upon guest release. (d) Pellets produced to estimate nominal density of samples, whose values considerably differ as a result of differences in porosity.

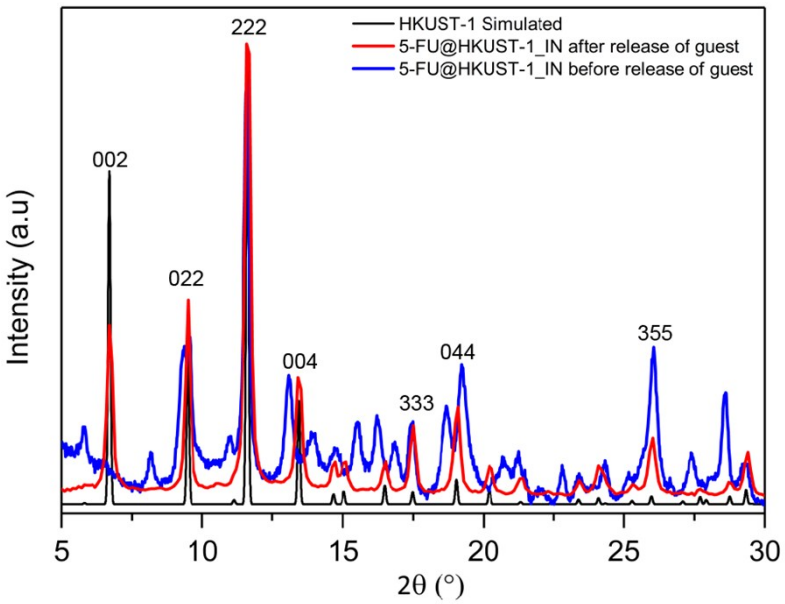

Fig. S2 Diffraction patterns of 5-FU@HKUST-1_IN before and after the release of the 5-FU (guest) drug molecules. Recovery of cubic symmetry is clear when comparison is made between the diffraction pattern of the host framework obtained after guest release and simulated pattern of HKUST-1. Labeling of Bragg peaks accompany the HKUST-1simulated pattern for reference.

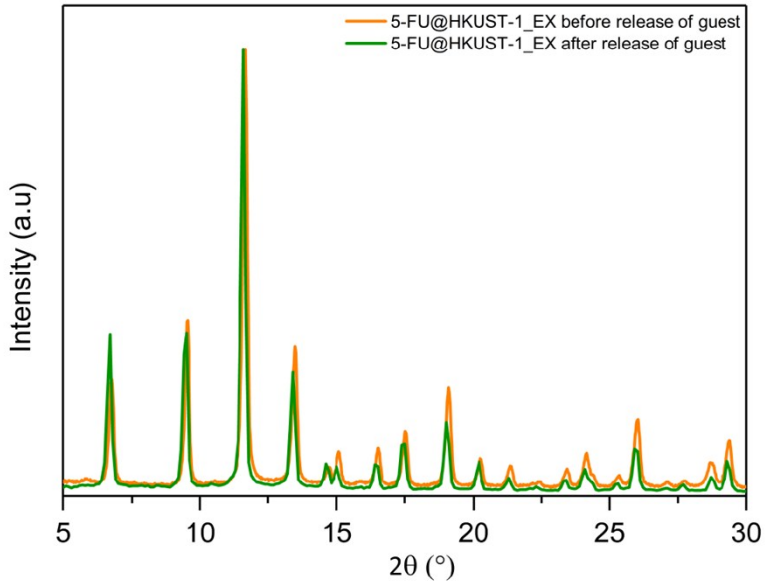

Fig. S3 Diffraction patterns of 5-FU@HKUST-1_EX before and after the release of the guest drug molecule. No apparent structural changes detected upon the release of 5-FU.

4. Confirmed guest release from host structure

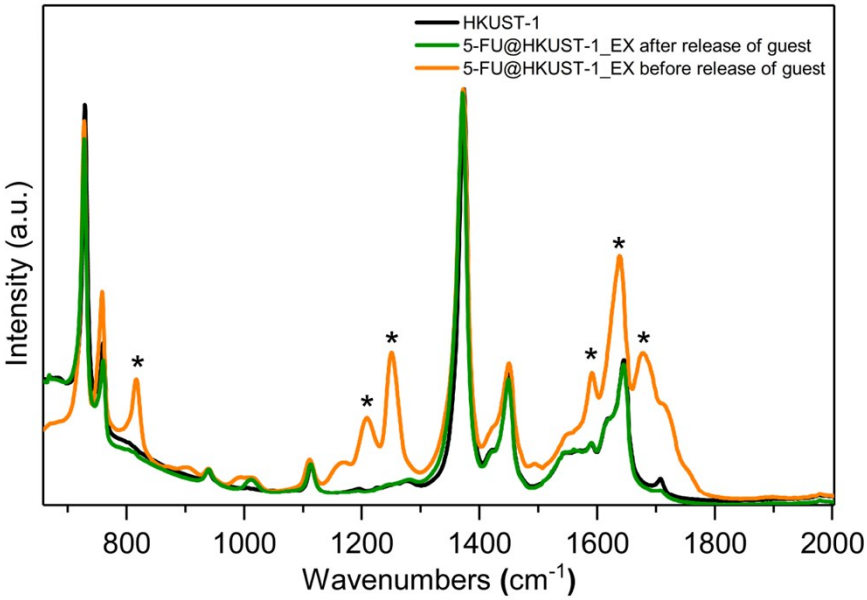

Fig. S4 ATR-FTIR spectra of 5-FU@HKUST-1_EX before and after the release of the guest drug molecule confirming the release of 5-FU. Asterisks mark the position of the 5-FU peaks.

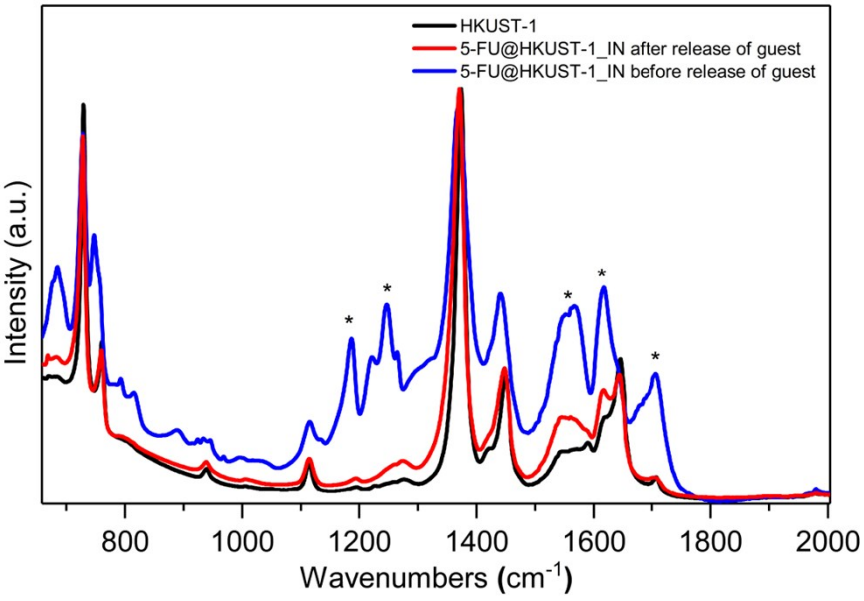

Fig. S5 ATR-FTIR spectra of 5-FU@HKUST-1_IN before and after the release of the guest drug molecule. The disappearance of the main 5-FU peaks shows the successful release of the drug molecule after sample was immersed in methanol and stirred for 72 hours. Asterisks mark the position of the 5-FU peaks.

5. Nitrogen adsorption/desorption isotherms

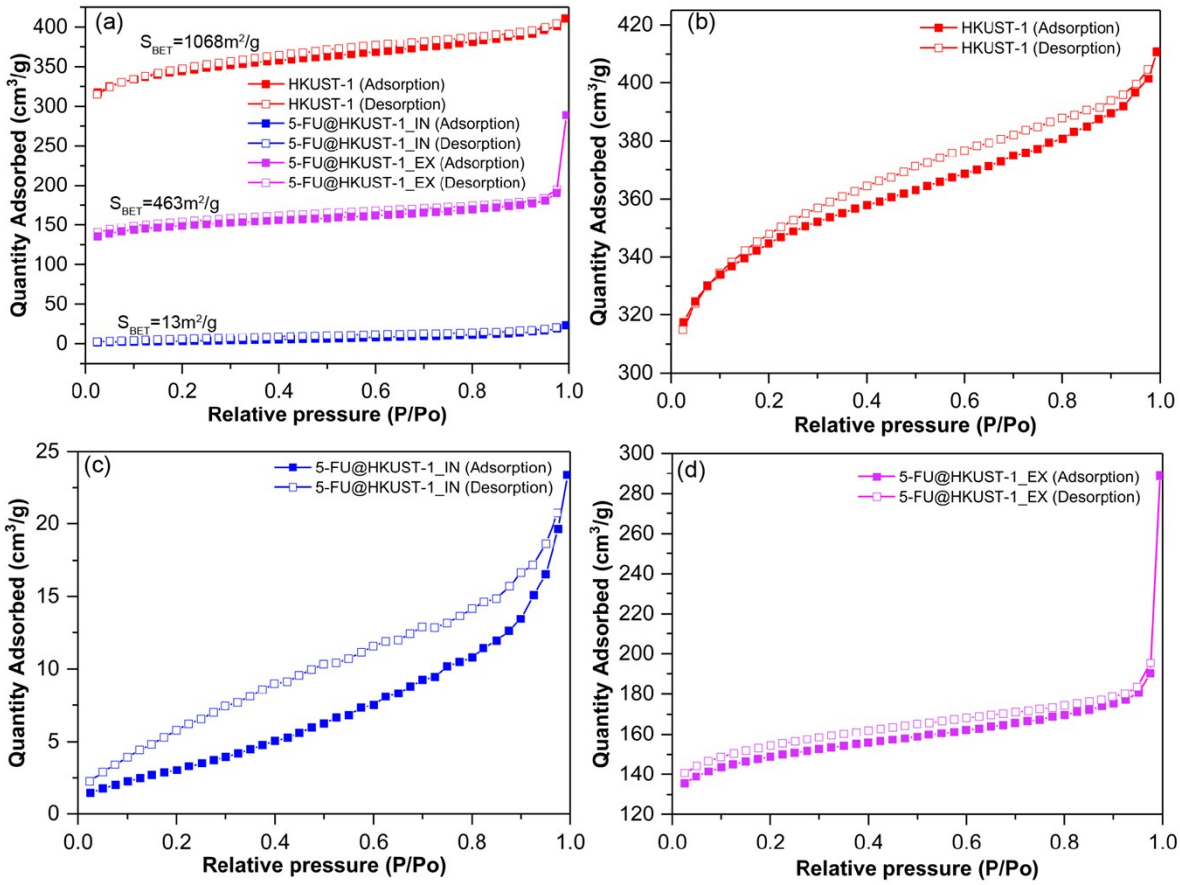

Fig. S6 a) Nitrogen adsorption and desorption isotherms of HKUST-1 and drug-loaded counterparts. Individual isotherms of b) HKUST-1, c) 5-FU@HKUST-1_IN and d) 5-FU@HKUST-1_EX. The HKUST-1 samples were activated at 90 °C under high vacuum for 12 hours prior to the N_2 adsorption measurements at 77K.

Table S2 Reported BET surface areas of HKUST-1 materials synthesised by mechanochemistry

	Method	Grinding time	BET surface area (m^2/g)	Reference
HKUST-1	Manual grinding	10 min	1068	This work
5-FU@HKUST-1_IN	Manual grinding	10 min	13	This work
5-FU@HKUST-1_EX	Manual grinding	10 min	463	This work
HKUST-1	Ball milling: neat grinding	30 min	1188	Li, Y., et al.[7]
	Grinding jar: neat grinding	20 min	1119	Schlesinger, M., et al[8]
	Grinding jar: assisted by solid solvent (NaCl)	20 min	1281	Yang, J., et al.[9]
	Extrusion: liquid assisted extrusion	-	1738	Crawford, D., et al.[10]
	Ball mill: liquid assisted grinding	25 min	758-1713	Klimakow, M., et al.[11]
	Kitchen grinder: liquid assisted grinding	5-60 min	707	Samal, M., et al.[12]
	Solvothermal	-	300-1500	Xiao, J., et al. [13]
	Solution-based	-	227	Li, Y., et al. [14]
	Solution-based	-	1564	Sofi, F. A., et al.[15]
	Solvothermal	-	629	Lestari, W. W., et al.[16]
	Electrochemical	-	324	Lestari, W. W., et al.[16]

6. Thermogravimetric analysis

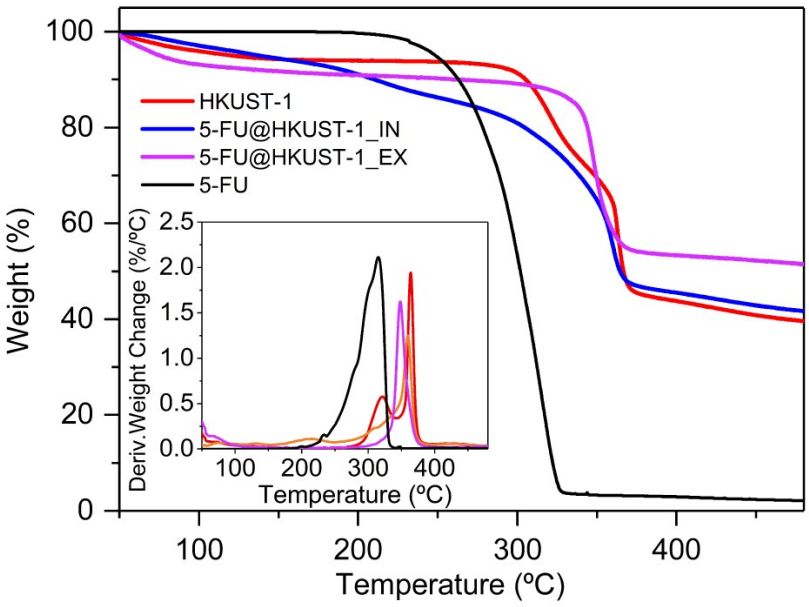

Fig. S7 TGA plots of HKUST-1 samples showing different material decomposition behavior as a function of temperature. Inset shows the derivative weight change with respect to temperature.

7. SEM and AFM images

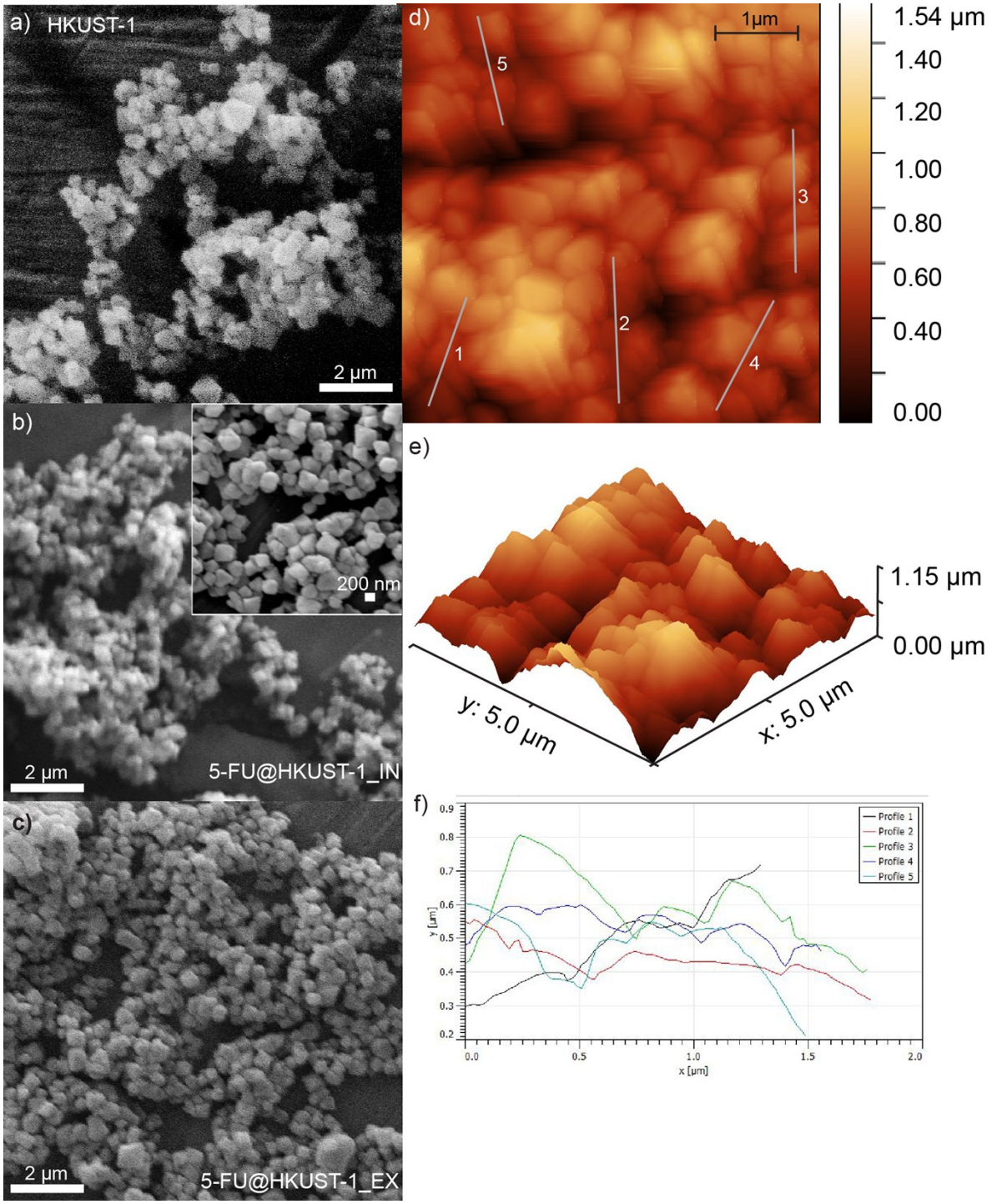

Fig. S8 SEM images of as synthesized (a) pristine HKUST-1, (b) 5-FU@HKUST-1_IN, and (c) 5-FU@HKUST-1_EX. The crystals show a uniform particle distribution, similar to the nanoHKUST-1 crystals fabricated *via* solution-based methods.[14] (d-e) AFM images of pristine HKUST-1 crystals for morphology characterization, accompanied by 3D representation of the surface topography. (f) Height profiles from traces marked in (d) for the calculation of crystal size of HKUST-1, which was found to be at 432 ± 83 nm (averaged of 100 measurements).

8. ATR-FTIR and INS data

Table S3 Characteristic vibrational bands of HKUST-1; units in cm^{-1}.

–Cu-O stretching	–C=C stretching of benzene ring	–OH bending	–C–O stretching	–C=O stretching of H_3BTC
728	1372	1448	1618	1706

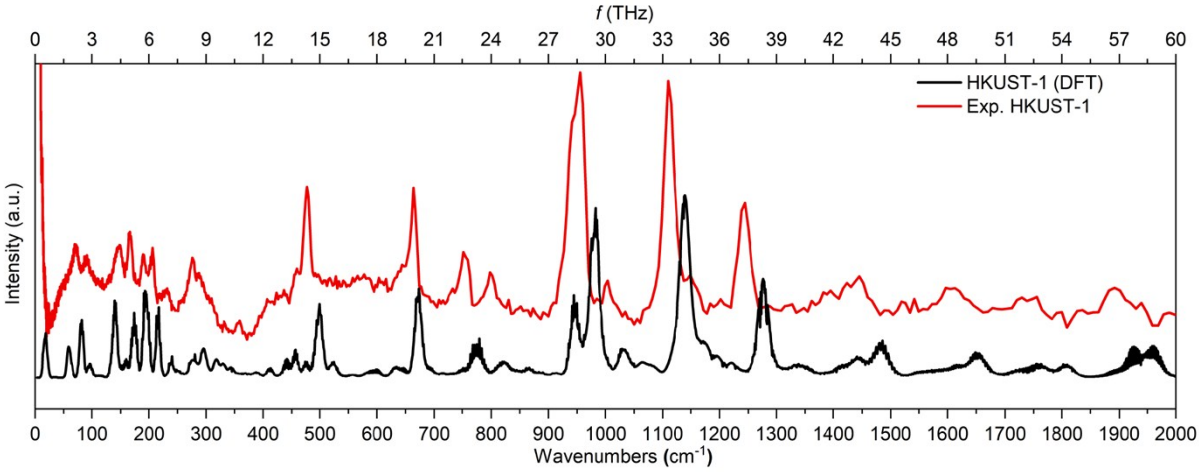

Fig. S9 Theoretical and experimental spectra of HKUST-1 for comparison. Theoretical spectrum is displayed in black and experimental spectrum is shown in red.

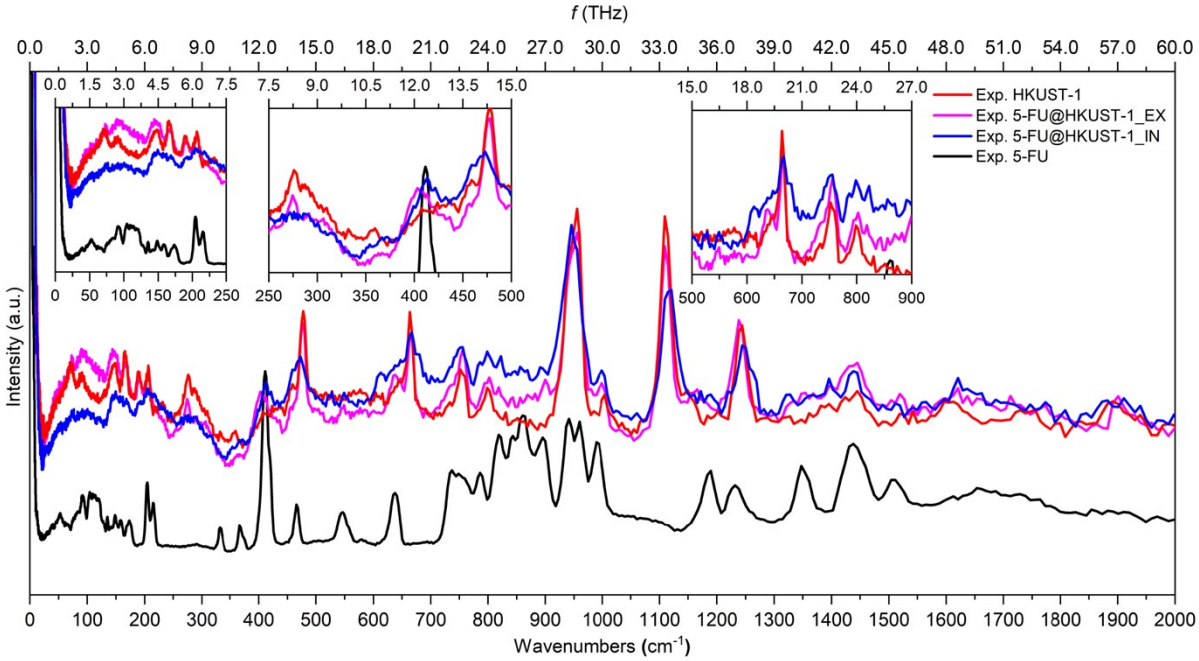

Fig. S10 Full INS spectra of HKUST-1 samples up to ~60 THz (2000 cm^{-1}). The experimental spectrum of 5-FU was scaled down by a factor of 5 to facilitate comparison with experimental data of HKUST-1.

Table S4 Description of vibrational and rotational modes of HKUST-1

Mode no.	Theo. (cm^{-1})	Exp. (cm^{-1})	Descriptions based on Ryder *et al.*[4]
0	19	(hidden)	Strong paddle wheel deformation and translational motion
1	60	70	Paddle wheel deformation and translational motion with organic linker rotation
2	83	91	Paddle wheel deformation and rotation with organic linker rocking
3	97	(hidden)	Organic linker trampoline-like motion
4	140	148	Paddle wheel rocking with organic linker rocking
5	160	(hidden)	Paddle wheel deformation
6	174	166	Paddle wheel translational motion
7	193	190	Asymmetric paddle wheel deformation (Cu-Cu buckling) with linker rocking
			Asymmetric paddle wheel deformation (O-Cu-O bending)
8	217	207	Paddle wheel rotation with strong linker rocking
9	241	232	Paddle wheel deformation (strong Cu-Cu buckling) with linker rocking
10	280	260	Asymmetric paddle wheel deformation (O-Cu-O bending and Cu-Cu buckling)
11	296	276	
12	318	288	Paddle wheel deformation with linker rocking
13	330	332	
14	345	359	
15	411	408	In Plane aromatic ring Rotation with Asymmetric Cu-O stretching
16	442	425	
17	457	438	
18	477	460	In Plane aromatic ring deformation with partially symmetric Cu-O stretching
19	499	478	Out of Plane aromatic ring deformation

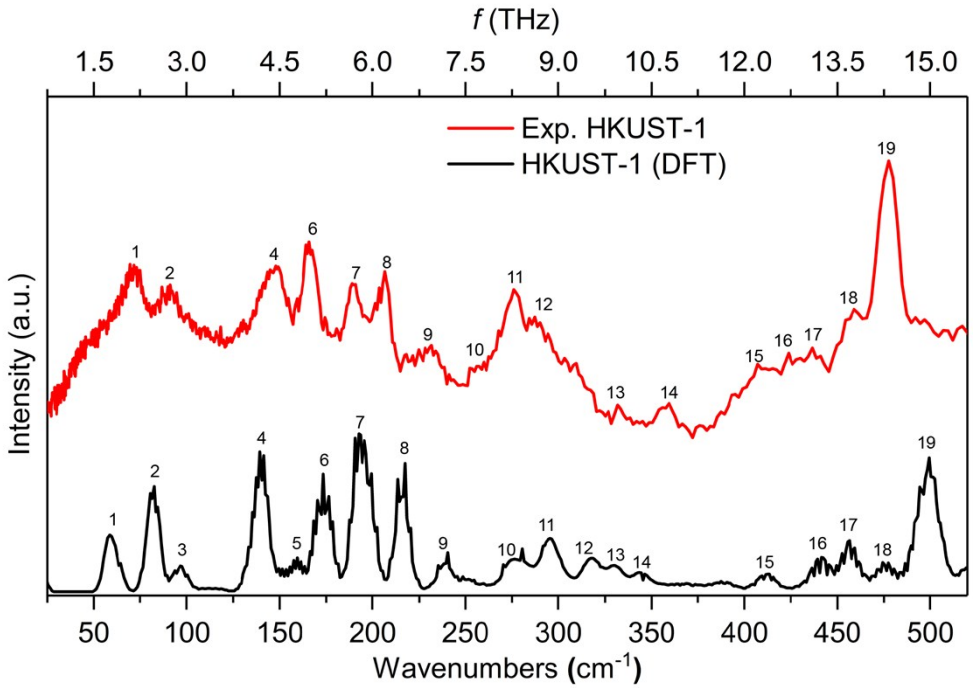

Fig. S11 Theoretical and experimental INS spectra of HKUST-1 with vibrational modes marked as #1-19 for easy correlation between theoretical and experimental data.

Table S5 Values of area under the inelastic curves and full width at half maximum (FWHM) values of the vibrational peaks of HKUST-1

	Wavenumber (cm^{-1})	Sample	Area under the graph ($S{\cdot}\omega$)	FWHM (cm^{-1})
	0-214	HKUST-1	504.8	-
		5-FU@HKUST-1_IN	402.6	-
		5-FU@HKUST-1_EX	477.9	-
Mode #6	155-175	HKUST-1	15.9	30.1
		5-FU@HKUST-1_IN	11.7	88.8
		5-FU@HKUST-1_EX	15.2	38.5
Mode #7	182-198	HKUST-1	11.9	44.7
		5-FU@HKUST-1_IN	9.1	139.3
		5-FU@HKUST-1_EX	10.9	39.05
Mode #8	198-217	HKUST-1	13.6	24.8
		5-FU@HKUST-1_IN	11.9	97.7
		5-FU@HKUST-1_EX	12.9	30.3
Mode #9	220-250	HKUST-1	17.8	66.5
		5-FU@HKUST-1_IN	16.5	83.5
		5-FU@HKUST-1_EX	15.2	68.6
Mode #11	269-282	HKUST-1	9.5	23.2
		5-FU@HKUST-1_IN	6.6	-
		5-FU@HKUST-1_EX	8.1	30.8
Organic linker deformation	465-489	HKUST-1	21.8	25.3
		5-FU@HKUST-1_IN	17.9	44.9
		5-FU@HKUST-1_EX	19.1	24.5

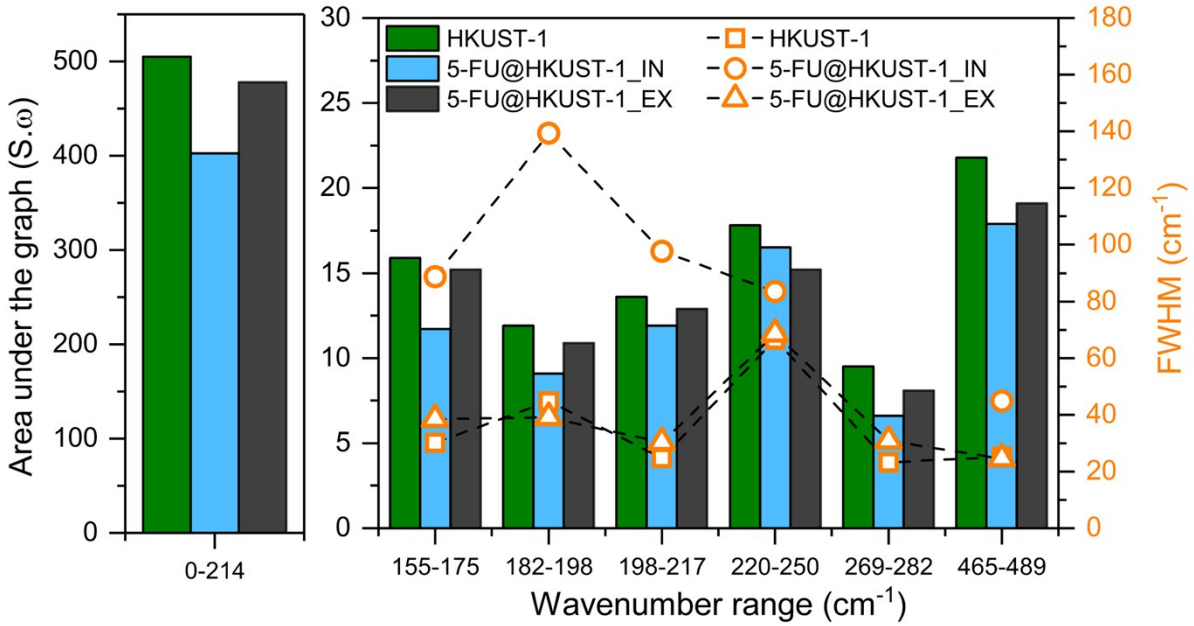

Fig. S12 Bar plot summarizing data presented in Table S5. The plot demonstrates the decrease in the area and the broadening of specific peaks related to copper (II) paddle-wheel vibrations in 5-FU@HKUST-1_IN sample.

References

1. S. F. Parker, F. Fernandez-Alonso, A. J. Ramirez-Cuesta, J. Tomkinson, S. Rudic, R. S. Pinna, G. Gorini and J. Fernández Castañon, *J. Phys. Conf. Ser.*, 2014, **554**.
2. O. Arnold, J. C. Bilheux, J. M. Borreguero, A. Buts, S. I. Campbell, L. Chapon, M. Doucet, N. Draper, R. Ferraz Leal, M. A. Gigg, V. E. Lynch, A. Markvardsen, D. J. Mikkelson, R. L. Mikkelson, R. Miller, K. Palmen, P. Parker, G. Passos, T. G. Perring, P. F. Peterson, S. Ren, M. A. Reuter, A. T. Savici, J. W. Taylor, R. J. Taylor, R. Tolchenov, W. Zhou and J. Zikovsky, *Nucl. Instrum. Meth. A*, 2014, **764**, 156-166.
3. R. S. Pinna, S. Rudić, S. F. Parker, J. Armstrong, M. Zanetti, G. Škoro, S. P. Waller, D. Zacek, C. A. Smith, M. J. Capstick, D. J. McPhail, D. E. Pooley, G. D. Howells, G. Gorini and F. Fernandez-Alonso, *Nucl. Instrum. Meth. A*, 2018, **896**, 68-74.
4. M. R. Ryder, B. Civalleri, G. Cinque and J.-C. Tan, *CrystEngComm*, 2016, **18**, 4303-4312.
5. S. F. P. K. Dymkowski, F. Fernandez-Alonso, *Phys. B Cond. Mat.*, 2018, DOI: 10.1016/j.physb.2018.02.034.
6. A. A. Talin, A. Centrone, A. C. Ford, M. E. Foster, V. Stavila, P. Haney, R. A. Kinney, V. Szalai, F. El Gabaly, H. P. Yoon, F. Leonard and M. D. Allendorf, *Science*, 2014, **343**, 66-69.
7. B. Yuan, X. Q. Yin, X. Q. Liu, X. Y. Li and L. B. Sun, *ACS Appl. Mater. Interfaces*, 2016, **8**, 16457-16464.
8. M. Schlesinger, S. Schulze, M. Hietschold and M. Mehring, *Microporous Mesoporous Mat.*, 2010, **132**, 121-127.
9. J. Yang, X. Feng, G. Lu, Y. Li, C. Mao, Z. Wen and W. Yuan, *Dalton Trans.*, 2018, **47**, 5065-5071.
10. D. Crawford, J. Casaban, R. Haydon, N. Giri, T. McNally and S. L. James, *Chem. Sci.*, 2015, **6**, 1645-1649.
11. M. Klimakow, P. Klobes, A. F. Thünemann, K. Rademann and F. Emmerling, *Chem. Mater.*, 2010, **22**, 5216-5221.
12. M. Samal, J. Panda, B. P. Biswal and R. Sahu, *CrystEngComm*, 2018, **20**, 2486-2490.
13. J. Xiao, Y. Zhu, S. Huddleston, P. Li, B. Xiao, O. K. Farha and G. A. Ameer, *ACS Nano*, 2018, **12**, 1023-1032.
14. Y. Li, X. Li, Q. Guan, C. Zhang, T. Xu, Y. Dong, X. Bai and W. Zhang, *Int. J. Nanomedicine*, 2017, **12**, 1465-1474.
15. F. A. Sofi, K. Majid and O. Mehraj, *J. Alloy Compd.*, 2018, **737**, 798-808.
16. W. W. Lestari, M. Adreane, C. Purnawan, H. Fansuri, N. Widiastuti and S. B. Rahardjo, *IOP Conference Series: Materials Science and Engineering*, 2016, **107**.